PROCEEDINGS OF ECOS 2023 - THE 36TH INTERNATIONAL CONFERENCE ON
EFFICIENCY, COST, OPTIMIZATION, SIMULATION AND ENVIRONMENTAL IMPACT OF ENERGY SYSTEMS
25-30 JUNE 2023, LAS PALMAS DE GRAN CANARIA, SPAIN

Modeling of a combined solar system including a thermal battery based on phase change material

Diane Le Roux[a], Sylvain Serra[b], Sabine Sochard[c], Zakaria Aketouane[d], Tessa Hubert[e], Ryad Bouzouidja[f], Alain Sempey[g] and Jean-Michel Reneaume[h]

[a] Universite de Pau et des Pays de l'Adour, E2S UPPA, LaTEP, Pau, France, diane.le-roux@univ-pau.fr, CA
[b] Universite de Pau et des Pays de l'Adour, E2S UPPA, LaTEP, Pau, France, sylvain.serra@univ-pau.fr
[c] Universite de Pau et des Pays de l'Adour, E2S UPPA, LaTEP, Pau, France, sabine.sochard@univ-pau.fr
[d] Nobatek/INEF 4, Anglet, France, zaketouane@nobatek.inef4.com
[e] Nobatek/INEF 4, Anglet, France, thubert@nobatek.inef4.com
[f] University of Bordeaux, CNRS UMR 5295, Arts et Metiers Institute of Technology, Bordeaux INP, INRAE, I2M Bordeaux, Talence, France, ryad.bouzouidja@u-bordeaux.fr
[g] University of Bordeaux, CNRS UMR 5295, Arts et Metiers Institute of Technology, Bordeaux INP, INRAE, I2M Bordeaux, Talence, France, alain.sempey@u-bordeaux.fr
[h] Universite de Pau et des Pays de l'Adour, E2S UPPA, LaTEP, Pau, France, jean-michel.reneaume@univ-pau.fr

Abstract:

Thermal energy storage (TES) is a key issue in efficient energy system applications, especially in the context of renewable energies. In this respect, phase change materials (PCM) have attracted interest as an active solution for efficient energy management, particularly in the building sector. This paper presents a modeling of a thermal battery based on PCM in the case of solar systems assisted by heat pump (SAHP). The storage tank allows to store the heat produced via unglazed solar panels (Batisol®) and represents the heat source of the heat pump. The heat pump can supply the heating and domestic hot water (DHW) needs of a building. The storage consists of a block of PCM contained between two plates of heat transfer fluid (HTF). A 2D model is used to describe the behaviour of the PCM and a 1D model is preferred for the HTF plates. The objective of the study is to dynamically simulate the thermal behaviour of this storage for different hot inlet temperature profiles: step, trapezoidal functions and profile of the temperature at the outlet of the thermal panels for a winter and summer period of 8 days. This 2D model would be useful to validate a simpler model for optimisation of the operational parameters of the system.

Keywords:

Thermal energy storage, Phase change material, Solar system assisted heat pump, Domestic hot water, Low-temperature heating.

1. Introduction

In order to limit temperature rise, it is important to reduce the environmental impact of energy production and consumption. According to the International Energy Agency [1], the building sector is considered to be one of the largest energy end-use sectors in the world. The growing demand for energy is increasing the pressure on the environment. One of the main challenges to reduce the environmental impact of buildings is therefore to replace fossil fuels with renewable resources. Thermal energy storage (TES) has been particularly studied in recent years as it is essential to compensate for the intermittency of renewable energies, by correcting the mismatch between energy supply and demand [2]. Moreover, TES are increasingly used to meet the heating and cooling needs of buildings. There are three types of TES: sensible, latent and thermochemical [2]. Phase Change Materials (PCM) are materials that can store large amounts of thermal energy in the form of latent heat of fusion when they change from a solid to a liquid state for example at a specific phase change temperature or temperature range if the PCM is not a pure compound. This phase transition process is reversible, allowing thermal energy to be stored and released at relatively constant temperatures. Compared to sensible heat storage materials, PCM offer several significant advantages, like a higher heat storage density at small temperature ranges [3]. PCM can store between 5 and 14 times more thermal energy per unit volume than sensible heat storage materials [4]. As a result, the use of PCM can help to reduce the size of heat storage systems, making them more suitable for residential applications. Thermochemical storage is more interesting in terms of storage density. However, this technology is less mature than that with PCM.

Solar systems assisted by heat pump (SAHP) can provide an efficient and environmentally friendly heating

https://doi.org/10.52202/069564-0189

and cooling solution for residential and commercial buildings. The role of a heat pump in the heating system is to increase the thermal energy from a lower temperature level to a higher temperature level [5]. Moreover, the use of PCM heat storage between the solar facade and the heat pump can improve the overall performance of the SAHP. Several studies have been conducted to assess the benefits of using PCM in SAHP [6–9]. Firstly, the solar energy stored in the PCM unit can be used as a heat source for the evaporator in the heat pump. As a result, the temperature of the evaporator is almost constant and the heat pump can operate under more stable conditions. This leads to a better Coefficient of Performance (COP) for the heat pump.

Depending on the type of application at the output of the heat pump (heating, cooling), the temperature levels are not the same and therefore the PCM used changes [6]. Four temperature ranges have been listed by Du *et al.* [6]: low (-20 to 5 °C), medium-low (5 to 40 °C), medium (40 to 80 °C) and high (80 to 200 °C) temperatures. For a heating or domestic hot water applications, the medium temperature level is considered since the buffer tank temperature setpoint is usually expected at 60 °C. Many studies have been carried out on such systems [6, 8–10]. However, as each storage is different (size, design and PCM used in particular), it is important to model its thermal behaviour correctly in order to explore the optimal operating parameters later.

The objective of this paper is to dynamically simulate a TES based on PCM integrated on SAHP. In a first part, the methodology and the case study will be presented. Then, several operating scenarios will be investigated in the results section. The profile of the hot temperature entering in the thermal battery will be a step, then a trapezoidal function, and finally this of the outler temperature of thermal panels in winter and summer periods using measured climatic conditions as boundaries. Finally, last part will conclude.

2. Material and Methods

This section is divided in three parts. Firstly, the global system is described, composed by solar thermal panels, PCM battery and heat pump. In next steps, the models of the different components of the system are defined. Dynamic models are based on the conservation of mass and energy equations.

2.1. Definition of the system

The studied system is composed of solar panels, a TES based on PCM, and a heat pump, as illustrated in Fig. 1. The system is divided in three circuits. The first, connecting the solar facade to the buffer tank, is made up of glycol. The second circuit, connecting the thermal battery to the heat pump, is composed of water. An air heater is integrated in parallel with the solar storage to supply heat to the heat pump when the temperature of the thermal battery is not high enough. The last circuit, also made of water, connects the PCM battery for heating and domestic hot water (DHW) to the heat pump.

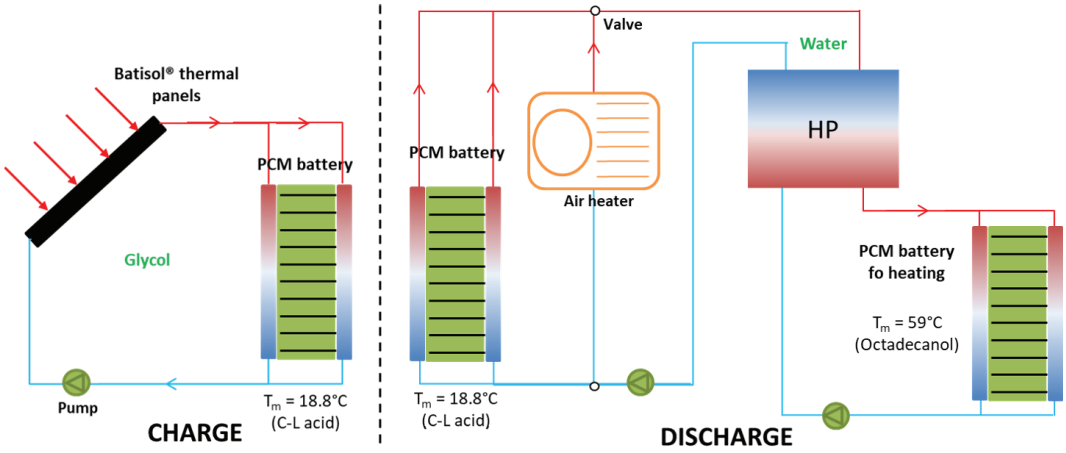

Figure 1: Global diagram of the solar assisted heat pump with thermal battery based on PCM.

The solar facade is composed of unglazed thermal panels (Batisol®) [11, 12], developed by Nobatek/INEF 4 [13]. The dimensions of the PCM-based storage are 0.4 m x 0.4 m x 0.4 m (Fig. 2a). The heat pump can produce both low temperature heating and DHW for a building application. The same thermal battery is used for the DHW and buffer tanks. Only the PCM changes between the two batteries, to match the desired temperature level. For the buffer tank, a mixture of 61.5% capric acid and 38.5% lauric acid (C-L acid) is used. Its melting temperature is 291.95 K. For the heating PCM battery, octadecanol is prefered. Indeed, its melting temperature is 332.46. The thermophysical properties of these materials are depicted in Table 1.

https://doi.org/10.52202/069564-0189

Table 1: Thermophysical properties of C-L acid [14] and octadecanol.

Name	Value for C-L acid	Value for octadecanol	Unit
T_m	291.95	332.46	K
L	$140.8 \cdot 10^3$	$208.45 \cdot 10^3$	J/kg
ρ_{PCM}	897.5	850	kg/m^3
$c_{p,l}$	1970	1750	$J/kg/K$
$c_{p,s}$	2240	2150	$J/kg/K$
λ_s	0.143	0.301	$W/m/K$
λ_l	0.139	0.205	$W/m/K$

2.2. Model of the Batisol® panels

The model of the thermal solar facade was described previously by Bouzouidja *et al.* [15]. From the time-varying input parameters, taken from a weather file, and the operating parameters, the temperature at the panel outlet is determined [15]:

$$T_{out,sol} = \frac{T_{in,sol} \cdot \dot{m} \cdot c_{p,H} + \alpha \cdot A_{sol} \cdot (0.5 \cdot T_{in,sol} - T_{ext}) + G_{sol} \cdot A_{sol} \cdot \gamma}{\dot{m} \cdot c_{p,H} - 0.5 \cdot \alpha \cdot A_{sol}} \tag{1}$$

Where $T_{in,sol}$ and T_{ext} are the temperatures at the entrance to the solar facade and outside (K), A_{sol} the surface of the solar facade (m^2), G_{sol} the solar flux (W/m^2), $\dot{m}$ the low rate of the Heat Transfer Fluid (HTF) circulating in the thermal panels (kg/s) and $c_{p,H}$ the specific heat capacity of the hot fluid (glycol) ($J/(kg \cdot K)$). The coefficients α and γ have been determined experimentally (γ = 0.63). The first one depends on the wind speed:

$$\alpha = -(7.84 + 3 \cdot v_{wind}) \tag{2}$$

2.3. Model of the thermal energy storage based on phase change material

In order to model the behaviour of latent heat storage, the following simplifying assumptions have been made:

- Natural convection is neglected. Only conduction is considered,
- No supercooling or superheating,
- Incompressible and Newtonian HTF,
- Kinetic and potential energy variations are neglected,
- Isothermal phase change (Octadecanol is a pure body so this assumption is correct. Since C-L acid is a mixture, the phase change temperature range is between 291.65 and 292.25 K [16]. As the melting temperature of this PCM is considered to be 291.95 K, the uncertainty of this assumption is +/- 2%),
- Density variation of PCM neglected during the phase change,
- Thermophysical properties are independent of temperature, but different for liquid and solid phases,
- The storage walls are assumed to be perfectly insulated (adiabatic boundary conditions) (Fig. 2b).

The shape of the thermal battery and its operation are described schematically in Fig. 2. The PCM is placed between two plates where the HTF circulates. Thus, a symmetry plane is visible in the middle of the battery. During the charging step, hot fluid is injected into the two plates. During the discharging step, cold fluid is injected. As a result, the charging and discharging steps are carried out separately. The plates where circulates the HTF are modelled in one dimension, a plug flow being assumed. The PCM part located between two plates is modelled in 2D because the heat diffusion operates in axial and longitudinal directions.

Fins are added to the plates to increase the contact area between the PCM and the HTF. To account for the fins, the effective conductivity of the PCM is expressed as:

$$\lambda_{eff} = a \cdot \lambda_{PCM} + (1 - a) \cdot \lambda_{fin} = a \cdot (\lambda_s + f_l \cdot (\lambda_l - \lambda_s)) + (1 - a) \cdot \lambda_{fin} \tag{3}$$

Where a is the proportion of PCM in the volume under consideration ($-$), λ_{PCM}, λ_s, λ_l et λ_{fin} are respectively the thermal conductivities of the PCM, the solid and liquid phases of the PCM and the fins ($W/m/K$), and f_l the liquid fraction of the PCM ($-$).

The enthalpy, the temperature and the liquid fraction of the PCM (according to x and y), and the temperature of the hot HTF (according to y) are determined with 4 to 11.

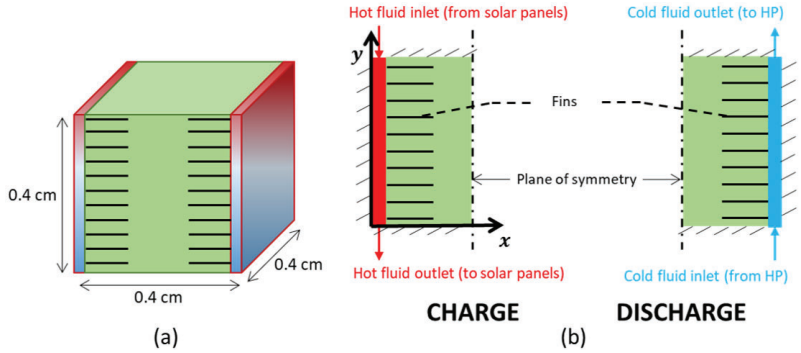

Figure 2: Diagram of the dimensions of the PCM-based thermal battery (a), and diagram of the PCM-based thermal battery with two plates for the charging and discharging steps (b).

- **Exchanges between the HTF (hot or cold) and the PCM:**

  For hot fluid:

$$\rho_H \cdot V \cdot c_{p,H} \frac{\partial T_H}{\partial t} - \dot{m}_H \cdot c_{p,H} \cdot \frac{\partial T_H}{\partial y} \cdot P = h_H \cdot A \cdot (T_H - T_{PCM}) + \lambda_H \cdot V \cdot \frac{\partial^2 T_H}{\partial y^2} \quad (4)$$

  For cold fluid:

$$\rho_C \cdot V \cdot c_{p,C} \frac{\partial T_C}{\partial t} + \dot{m}_C \cdot c_{p,C} \cdot \frac{\partial T_C}{\partial y} \cdot P = h_C \cdot A \cdot (T_C - T_{PCM}) + \lambda_C \cdot V \cdot \frac{\partial^2 T_C}{\partial y^2} \quad (5)$$

- **Exchanges in the PCM:**

$$\frac{\partial H_{PCM}}{\partial t} = \frac{\partial \lambda_{eff}}{\partial x} \cdot \frac{\partial T_{PCM}}{\partial x} + \frac{\partial \lambda_{eff}}{\partial y} \cdot \frac{\partial T_{PCM}}{\partial y} + \lambda_{eff} \cdot \frac{\partial^2 T_{PCM}}{\partial x^2} + \lambda_{eff} \cdot \frac{\partial^2 T_{PCM}}{\partial y^2} \quad (6)$$

$$H_{PCM}(T_{PCM}) = f_l \cdot H_l + (1 - f_l) \cdot H_s = \rho_{PCM} \cdot ((c_{p,s} + f_l \cdot (c_{p,l} - c_{p,s})) \cdot T_{PCM} + L \cdot f_l - f_l \cdot (c_{p,s} + f_l \cdot (c_{p,l} - c_{p,s})) \cdot T_m) \quad (7)$$

$$f_l = \begin{cases} 0 & for\ H_{PCM} < H_s \\ \frac{H_{PCM} - H_s}{H_l - H_s} & \\ 1 & for\ H_{PCM} > H_l \end{cases} \quad (8)$$

- **Boundary conditions for the PCM in contact with hot (during charging step) or cold (during discharging step) HTF:**

  For hot fluid (for x = 0 and 0.4 m):

$$h_H \cdot (T_H - T_{PCM}) = -\lambda_{eff} \frac{\partial T_{PCM}}{\partial x} \ for\ x = 0\ m \quad and \quad h_H \cdot (T_H - T_{PCM}) = \lambda_{eff} \frac{\partial T_{PCM}}{\partial x} \ for\ x = 0.4\ m \quad (9)$$

  For cold fluid (for x = 0 and 0.4 m):

$$h_C \cdot (T_C - T_{PCM}) = -\lambda_{eff} \frac{\partial T_{PCM}}{\partial x} \ for\ x = 0\ m \quad and \quad h_C \cdot (T_C - T_{PCM}) = \lambda_{eff} \frac{\partial T_{PCM}}{\partial x} \ for\ x = 0.4\ m \quad (10)$$

- **Boundary conditions for the PCM in contact with the outside (adiabatic conditions):**

$$\lambda_{eff} \frac{\partial T_{PCM}}{\partial y} = 0 \ for\ y = 0 \ and\ 0.4\ m \quad (11)$$

- **Initial conditions:** All temperatures are fixed at 283.15 K. The enthalpy of the PCM is determined by 7 at 283.15 K. The liquid fraction is considered equal to 0.

https://doi.org/10.52202/069564-0189

Where h_H and h_C are the convective exchange coefficients of the hot and cold fluid respectively ($W/m^2/K$), T_H, T_C, T_{PCM} and T_m are the hot and cold temperature, the temperature of the PCM and the melting temperature of the PCM, L the latent heat (J/kg), ρ_{MCP} the PCM density (kg/m^3), $c_{p,l}$ and $c_{p,s}$ are the specific heat capacity of the liquid and solid phases respectively ($J/kg/K$), P the exchange perimeter (m), A the exchange area (m^2) and V the volume of the representative element considered (m^3). The convective exchange coefficients are determined from the Nusselt number, assuming that the wall thickness of the plate is very thin and therefore negligible.

The boundary conditions of the thermal battery depend on the configuration studied. Four scenarios have been investigated. Firstly, the profile of hot temperature entering the thermal battery follows a step. In a second stage, it is a trapezoidal function. Finally, the battery based on PCM is connected to the Batisol® panels and two periods of 8 days are simulated: winter (from January 1 to 8) and summer (from July 1 to 8). In the latter two cases, the profile of the outlet temperature of the solar panels is used as input to the PCM:

$$T_H(x, y = 0.4, t) = T_{out,sol} \tag{12}$$

2.4. Resolution of the differential algebraic equations and software used

The software used to model the system is OpenModelica v1.18.0. The Modelica library (v3.2.3) is considered. The spatial discretisation is performed manually while the temporal discretisation is performed via the DASSL integrator available on OpenModelica. The tolerance used in the DASSL integrator is 10^{-6}. For the PCM-battery model, equations are discretised using an explicit second-order discretisation scheme with finite differences. For the boundary conditions (9 to 11), second-order decentred schemes are used.

3. Results and Discussion

This section is divided into three parts. The first one aims at studying the behaviour of PCM-based TES for a hot inlet temperature profile following a ramp (case 1). The second part investigates the behaviour of the system under trapezoidal loads (case 2). Finally, the battery is connected to the Batisol® solar facade and an 8-day simulation is performed for two periods of the year: from 1 to 8 January (winter, case 3) and from 1 to 8 July (summer, case 4). The hot HTF temperatures investigated at the buffer tank inlet are shown in Fig. 3. The colours red, green, blue and yellow refer to cases 1, 2, 3 and 4 respectively. For the next figures, the coordinates (x = y = 0 m) are placed at the bottom left of the PCM in Fig. 2.

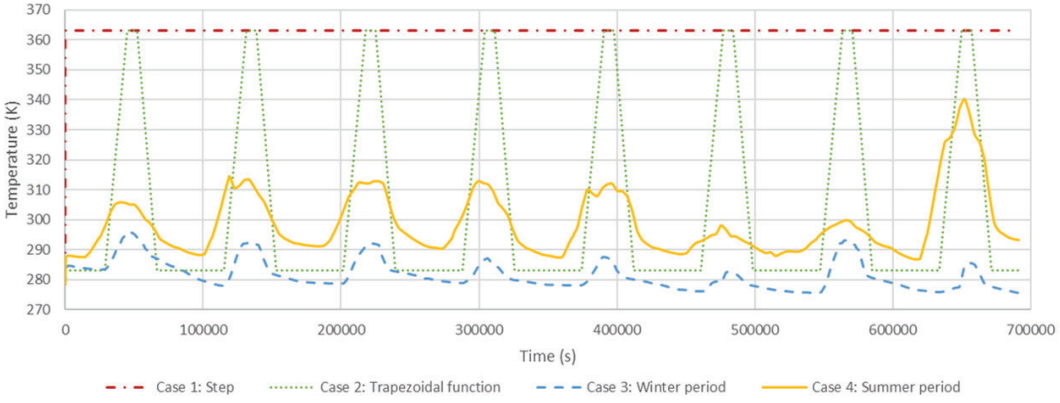

Figure 3: Four hot temperatures profiles considered at the input of the PCM-based TES battery.

The simulation times are relatively fast for simulating 8 days ($6.912 \cdot 10^{-5}$ s) on a standard laptop (processor: 12th Gen Intel®Core(TM) i7-12700H 2.69 GHz and RAM: 32 Go). They amount to 30 s and 2 min for cases 1 and 2 respectively. When the weather file is used and the Batisol® thermal panel model is added, the simulation times are slightly longer but remain below 5 min.

3.1. Profile of the hot inlet temperature following a step

For the case 1, the input temperature profile follows a ramp from 283.15 to 363.15 K in the first second of the simulation. The evolution of the liquid fraction and the temperature of the PCM in the tank are studied in Fig. 4 over time for the first slice of PCM in contact with the hot plate (for x = 0 m), according to the vertical. The colours purple, green and red refer to the high (y = 0.4 m), middle (y = 0.2 m) and low (y = 0 m) parts of the PCM respectively. Solid lines are used for the temperature and dashed lines are preferred for the liquid fraction. The same marking and colour code will be used in the following sections. Initially, the PCM is in the solid state

(f_l = 0) at 283.15 K. Its temperature increases until it reaches the melting temperature (291.95 K) at 18.2 s for y = 18 (in purple), the top of the PCM in contact with the hot plate. This temperature is reached at 20.8 s for the middle of the PCM (in green), and 23.2 s for the bottom of the PCM (in red). From these times onwards, the temperature of the PCM remains constant while the liquid fraction increases until it reaches unity, indicating that all the PCM has changed from the solid to the liquid state. This event occurs at 78.0, 82.1 and 87.5 s for the top, middle and bottom of the PCM respectively. From then on, the liquid fraction remains constant and the temperature of the PCM gradually increases, while approaching the temperature of the hot HTF.

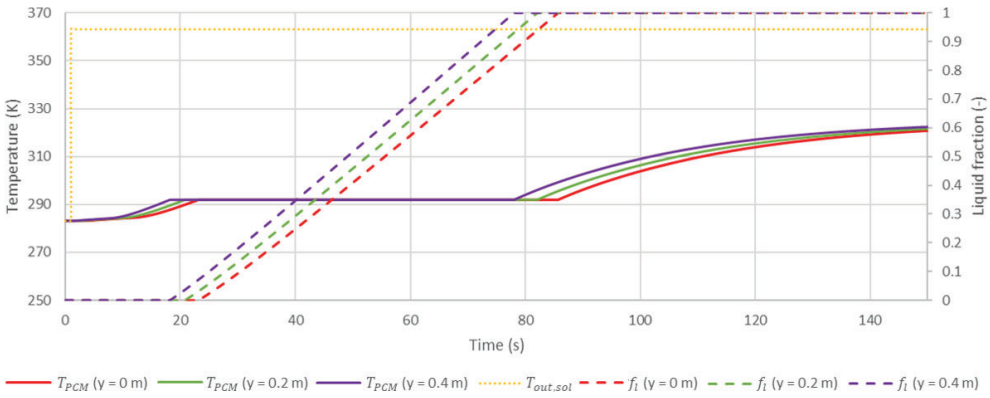

Figure 4: Case 1: Temperature and liquid fraction evolution for the first PCM layer in contact with the hot plate (x = 0 m) and for y = 0, 0.2 and 0.4 m.

The evolution of these two variables has also been studied for different values of x in Fig. 5. As the battery is symmetrical, only the coordinates at x = 0 (in red), 0.06 (in yellow) and 0.2 m (in green) are presented for the sake of clarity. In this case, the profiles are clearly different. The phase change from solid to liquid state is clearly visible for the first layer in contact with the hot plate. For x = 0.06 m, the temperature evolves linearly without reaching the melting temperature. As a result, the liquid fraction remains constant and equal to zero. For the PCM in the middle of the battery (x = 0.2 m), the temperature remains almost constant (283.15 K), indicating that the heat has not reached the core of the battery in 150 s.

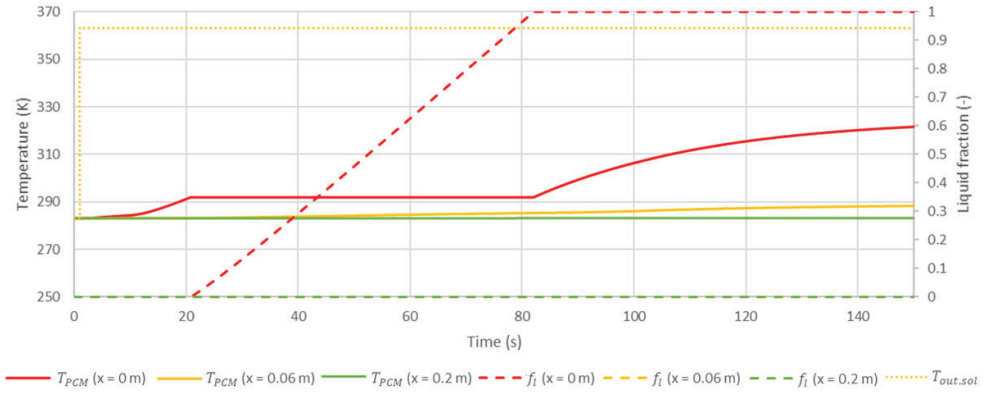

Figure 5: Case 1: Temperature and liquid fraction evolution in the longitudinal direction (for x = 0, 0.06 and 0.2 m) for the PCM layer in the middle (y = 0.2 m).

Figures 4 and 5 show the interest of considering a 2D model for PCM tank, according to longitudinal (x) and vertical (y) directions, since the temperatures in the PCM are different in both directions.

3.2. Profile of the hot inlet temperature following a trapezoidal function

Before studying the thermal behaviour of the storage connected to the solar facade, a trapezoidal function is used to simulate the evolution of the hot temperature at the battery inlet (Fig. 3). The period of this function is decomposed on 28800 s of width, 16200 s of rising , 7200 s of width, 14400 s of falling, for a total period of 86400 s. The temperature and liquid fraction are studied as before, for the first slice in contact with the hot

https://doi.org/10.52202/069564-0189

plate (for x = 0 m) (Fig. 6), and the slice in the middle of the PCM (for y = 0.2 m) (Fig. 7). The same evolution as for the ramping test is observed. In a first step, the temperature of the PCM increases until it reaches the melting temperature of the PCM (at 30634 s) (Fig. 6a). Then the liquid fraction increases until it reaches unity (Fig. 6b). At this point (31049 s), the temperature of the PCM increases again (Fig. 6a). The temperature of the PCM follows the temperature of the hot HTF at the battery inlet, with an average difference of less than 6%. In order to store as much heat as possible and not send it to the solar circuit, it can be interesting to stop the charging step when the temperature of the PCM becomes higher than that of the hot coolant. Figure 6 shows that this moment occurs at 52200 s.

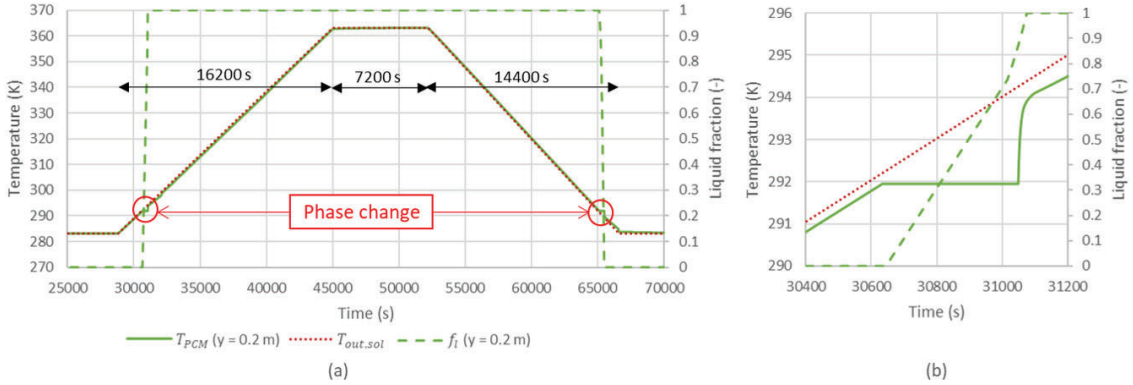

Figure 6: Case 2: Temperature and liquid fraction evolution for the first PCM layer in contact with the hot plate (x = 0 m) and for y = 0.2 m (a), focus on the phase change between 30634 and 31049 s (b).

Figure 7a shows the evolution of the temperature and liquid fraction of the PCM in the longitudinal direction (x = 0, 0.06 and 0.2 m) for the PCM layer at y = 0.2 m. The difference in temperature is clearly visible for the three curves. The further the PCM is from the hot plates, the lower its temperature and the longer the phase change takes. The heat propagation is thus clearly visible along the PCM. The core of the PCM (x = 0.2 m in green) takes the longest time to melt, but also to solidify as the hot inlet temperature decreases. The change from liquid to solid state is thus much longer (13 times longer) than for the PCM layers closer to the hot plate. For the yellow curve (x = 0.06 m), after the phase change, slight instabilities are visible in the PCM temperature. This must be due to the discretisation step and/or the discretisation scheme, whose order should be increased to be more accurate, and/or the DASSL integrator whose tolerance must be increased. The phase change step is significantly larger for x = 0.2 m. This is because the heat propagates from layer to layer. During the phase change of a PCM layer, all the energy required to achieve the phase change is absorbed. Therefore, for the liquid fraction of the layer x = 0.2 m to fluctuate, the liquid fractions of the previous layers must already have reached an equilibrium (solid or liquid state). This is illustrated in Fig. 7b, which shows a zoom of the transition from solid to liquid state (between 31000 and 35000 s) for the layers x = 0 (in red), 0.02 (in purple), 0.04 (in blue) and 0.06 m (in yellow). It can be seen that the liquid fraction of the next layer increases when the liquid fraction of the layer under consideration has reached 1. As a result, even if the melting temperature of the PCM has been reached for a PCM layer, it is necessary to wait until the change of state has taken place in the layers closer to the hot plates before the phase change begins in the PCM layer.

3.3. Profile of the hot inlet temperature following the outlet temperature of the Batisol® panels

When the PCM-based storage is connected to the Batisol® thermal panels, the temperature of the inlet hot HTF is calculated by 1. The surface area of the thermal panels is 25.5 m^2 (5 m wide by 5.1 m long). The surface area consists of 16 panels with 24 channels. Meteorological data from Cholet (next to Nantes) in 2021, in the northwest of France, are used. Figure 8 presents the evolution of the solar power and the outdoor temperature for the 2 periods (winter and summer) considered. The solar power amounts to 112 W/m^2 over the 8 winter days considered, whereas over the summer period considered this value is 2.5 times higher. The average outdoor temperature is 280 K and in summer 291.83 K. These two periods were chosen to represent different types of days, with more or less sunshine and wind, cold or hot outside temperatures (Fig. 8). In addition, 8-day periods were considered in order to determine the capacity of the battery to store heat during renewable energy intermittencies and day/night alternations.

https://doi.org/10.52202/069564-0189

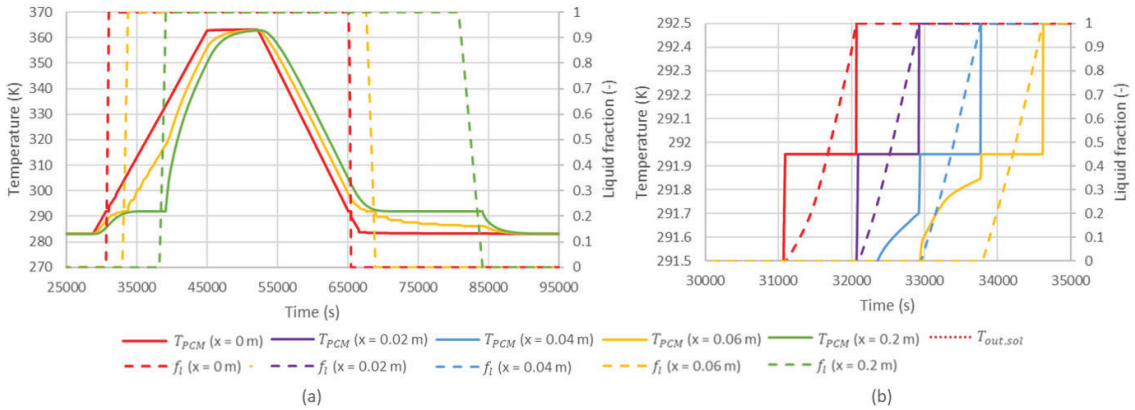

Figure 7: Case 2: Temperature and liquid fraction evolution in the longitudinal direction (for x = 0, 0.06 and 0.2 m) for the PCM layer in the middle (y = 0.2 m) (a), focus on the phase change of the first four PCM layer (from x = 0 to 0.06 m) (b).

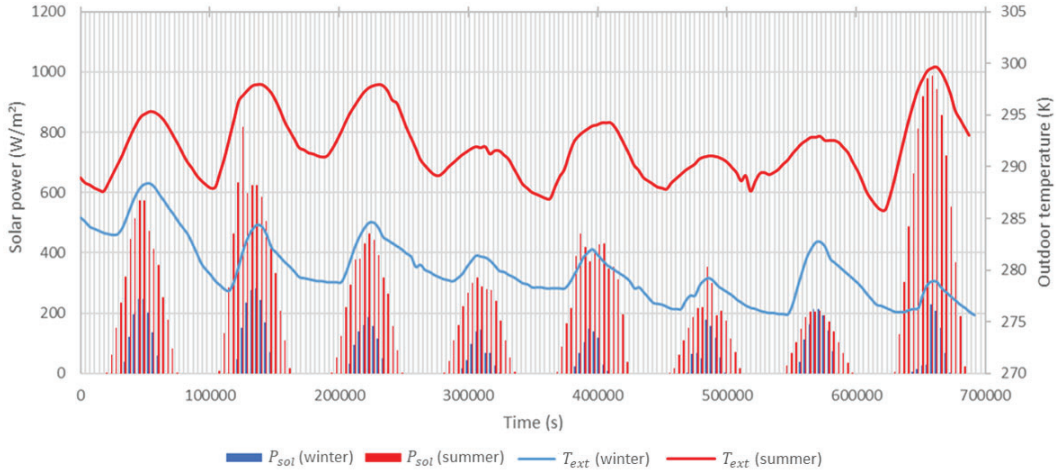

Figure 8: Cases 3 and 4: Evolution of solar power and outdoor temperature over the 8 days studied in winter and summer.

3.3.1. Winter period

The winter period chosen to simulate the behaviour of the PCM battery is from January 1 at 0am to January 8 at 23pm. In order to simplify the understanding of the graphs over longer periods (8 days), only the temperature and liquid fraction of the middle cell (y = 0.2 m) of the layer in contact with the hot plate (x = 0 m) are considered in Fig. 9. Over the 8 days simulated, the temperature at the exit of the solar facade is only higher than the melting temperature of the PCM on four days (Fig. 3). The PCM temperature exceeds the melting temperature only on January 1, 2, 3 and 7, as shown in Fig. 9. Indeed, the liquid fraction remains zero except between 11.15am and 4.5pm on January 1st, between 12.4pm and 16pm on January 2, between 14pm and 15.15pm on January 3, between and 13pm and 15.5pm on January 7. On other days, the PCM never reaches the melting temperature. Nevertheless, heat is stored in the solid state, as with sensible TES but with low efficiency. Fig. 9 shows that it is important to choose a material with a melting temperature that is not too high in order to take advantage of the phase change. If the melting temperature was 298.15 K (291.95 K for C-L acid), the PCM would not have changed state during the winter period under consideration. As a result, the use of PCM-based storage would not be interesting.

The temperature of the PCM in contact with the hot plate is almost as high as that of the hot HTF at the inlet, with an average difference of 0.3% over the 8 days. Figure 10a shows the evolution of the temperature and liquid fraction for the PCM layer at y = 0.2 m and for x = 0 (in red), 0.06 (in yellow) and 0.2 m (in green). As seen earlier, the temperatures are lower and lower from the outside of the PCM towards the inside. Indeed,

https://doi.org/10.52202/069564-0189

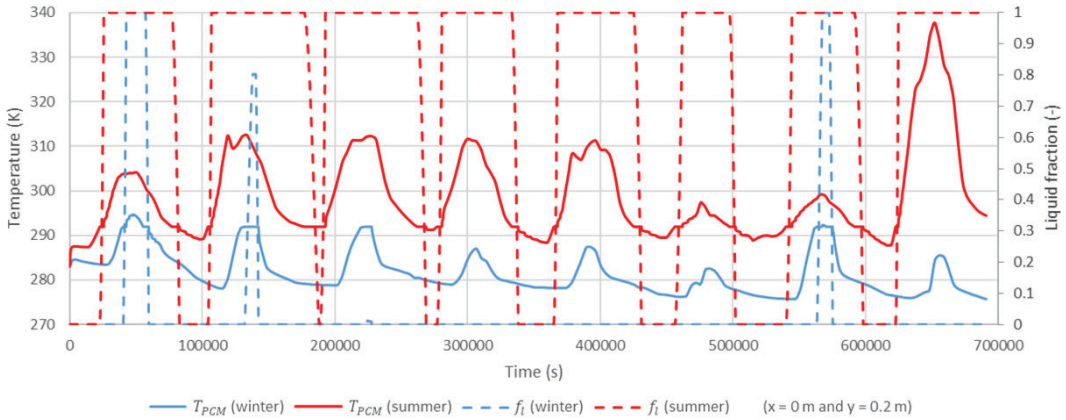

Figure 9: Cases 3 and 4: Temperature and liquid fraction evolution for the first PCM layer in contact with the hot plate (x = 0 m) and for y = 0.2 m.

the green curves show that the PCM has not changed state in the middle of the thermal battery. Furthermore, Fig. 10 shows the heat propagation along the PCM, with lower temperatures at the ends of the PCM, after the hot temperature at the inlet is decreased (after 60000 s). In general, the heat propagates well in the PCM, since the temperature differences between the different layers of PCM in the hot HTF are less than 0.8%. The instabilities visible at x = 0 and 0.06 m are due to the slight change in temperature at the outlet of the thermal panels (red dotted line in Fig. 10a), which of course depends on the weather conditions. These instabilities appear at the extremities of the PCM close to the hot plates (such as at x = 0 and 0.06 m) but not at the centre of the PCM (at x = 0.2 m). As seen previously, the liquid fraction of the x = 0.2 m layer remains zero while the melting temperature has been reached (291.95 K at 53100 s). This is due to the liquid fractions of the layers closer to the hot plate, which have not all reached unity. The output temperature of the solar panels decreases from 47483 s onwards, and consequently the energy supplied to the PCM. As a result, the middle layer (x = 0.2 m) has not received enough energy to make its phase change. Figure 10b is a zoom of the phase change (solid to liquid) in Fig. 10a. Before a layer changes phase, it is necessary that the liquid fraction of the previous layer has reached unity. Figure 10b shows this clearly, with the increase from 0 to 1 in the liquid fraction at x = 0 m (38900 to 40440 s), then that at x = 0.02 s (40440 to 42747 s), then that at x = 0.04 m (42747 to 44826 s) and finally that at x = 0.06 m (44826 to 47470 s).

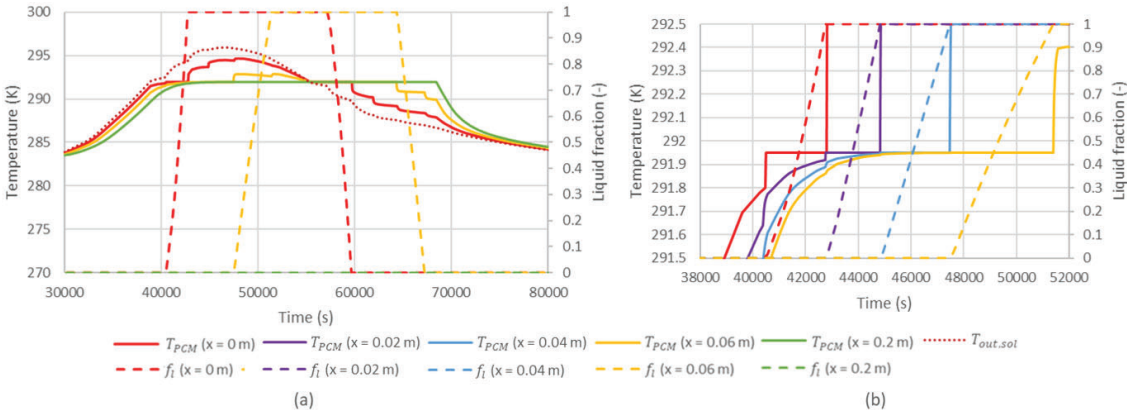

Figure 10: Case 3: Temperature and liquid fraction evolution in the longitudinal direction (for x = 0, 0.06 and 0.2 m) for the PCM layer in the middle (y = 0.2 m) (a), focus on the phase change of the first four PCM layer (from x = 0 to 0.06 m) (b).

3.3.2. Summer period

The summer period chosen to simulate the behaviour of the PCM battery is from July 1 at 0am to January 8 at 23pm. The temperature and liquid fraction at x = 0 m and y = 0.2 m are shown in the same figure as the winter period (Fig. 9). The temperature of the hot HTF at the storage inlet is significantly higher than during the winter

period (up to 340 K vs 296 K as illustrated in Fig. 3). The differences between the maximum temperatures expected by the hot fluid at the outlet of the thermal panels range from 2% (January 7 and July 7) to 16% (January 8 and July 8). On average the temperatures are 8% higher in summer. As a result, the behaviour of the PCM is also different between winter and summer periods, with phase changes occurring less often in winter. The advantage of using PCM in summer is therefore much greater, since it is possible to limit the size of the battery thanks to the change in the state of the material, unlike the use of sensible storage. Even on less sunny days such as July 6, when the temperature of the hot HTF does not exceed 297 K, there is enough heat to allow the PCM to change state. The PCM remains in a liquid state longer than in winter, between 7am and midnight on average over the 8 days considered.

As for the winter period, the difference between the temperature of the PCM in contact with the plate and that of the hot HTF is small (0.5% difference on average over the 8 days). Figure 11a shows the evolution of the temperature and liquid fraction for the PCM layer at y = 0.2 m and for x = 0. (in red), 0.06 (in yellow) and 0.2 m (in green). The temperature differences from the outside to the inside of the PCM are also clearly visible. From 16.4pm onwards, the temperature of the PCM in the core of the battery is higher than that of the PCM in contact with the hot plate. It would therefore be interesting to stop the charging step and start the discharging step by switching the hot (solar system) and cold (heat pump) inputs. The same instabilities as for winter period appear in Fig. 11a for the same reasons (small fluctuations of the temperature at the outlet of the thermal panels due to climatic conditions). The phase change zoom of the first four layers is illustrated in Fig. 11b (for x = 0 (in red), 0.02 (in purple), 0.04 (in blue) and 0.06 m (in yellow)).

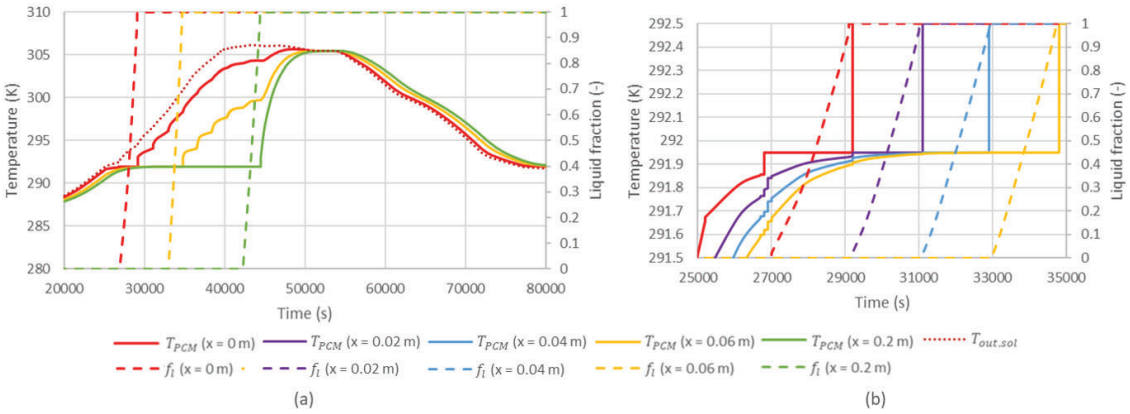

Figure 11: Case 4: Temperature and liquid fraction evolution in the longitudinal direction (for x = 0, 0.06 and 0.2 m) for the PCM layer in the middle (y = 0.2 m) (a), focus on the phase change of the first four PCM layers (from x = 0 to 0.06 m) (b).

The energy stored by the thermal battery for the two periods considered (winter and summer) is given in Table 2. During the winter period under consideration, the average stored energy is 164 Wh per day. In summer, this value is 6 times higher. The sunniest days (January 1st in winter and July 8 in summer) store 5 to 7.5 times more energy than the days less suitable for thermal collectors (January 6 and July 6). On average, the PCM battery can store 2.6 kWh/m^3 per day of energy in winter and 6.6 kWh/m^3 for January 1st. In summer this value reaches 15.1 kWh/m^3 per day on average and 29.3 kWh/m^3 for July 8. The benefit of PCM is clearly visible in summer, with almost 6 times more energy stored by the battery than in winter, partly due to the more frequent phase changes.

Table 2: Energy stored in the thermal battery per day (Wh).

Period	Minimal value	Maximal value	Mean
Winter	56 (January 6)	423 (January 1st)	164
Summer	385 (July 6)	1877 (July 8)	964

4. Conclusion

A dynamic model of a SAHP based on the use of thermal panels (Batisol®) and a latent heat storage was presented. This system aims to provide the heating and domestic hot water needs of a building. The TES is

https://doi.org/10.52202/069564-0189

composed of a PCM contained between two plates where HTF circulate. During the charging step, the hot HTF is fed by the thermal panels. During the discharging step, the direction of the fluid is reversed and the cold HTF is fed by the heat pump.

The thermal behaviour of the PCM tank is studied for four different profiles of the charging temperature: ramping, trapezoidal functions, temperature at the outlet of the thermal panels in winter (from January 1 to 8) and in summer (from July 1 to 8). The simulations carried out in OpenModelica showed the behaviour of the PCM during the phase change. The developed model showed the importance of choosing a PCM with a melting temperature range suitable for the studied application. In winter, only the sunniest days allows the PCM to melt while in summer the phase change occurs every day. On average, this thermal battery can store 6.6 and 15.1 kWh/m^3 per day of energy in winter and summer respectively.

The simulations showed that the 2D model of the system is necessary to take into account the horizontal and vertical temperature variations in the battery. This model will be further validated with experimental data. It will also allow the development and the validation of a simpler model. The final goal will be to optimise the SAHP system on its operational parameters with the simpler model.

Acknowledgments

This work was supported in the case of MCPBat project granted by the Region Nouvelle Aquitaine. Grant number 11385520-11389020 in the framework of the joint research team between the University of Pau and Pays de l'Ardour and Nobatek/INEF4.

Nomenclature

Letter symbols

- a proportion of PCM in the volume considered,
- A exchange surface, m^2
- c_p specific capacity, $J/(kgK)$
- f_l liquid fraction,
- G_{sol} solar flux, W/m^2
- h heat transfer coefficient, W/m^2K
- H enthalpy (including sensible and latent forms), J/m^3
- L latent heat, J/kg
- $\dot{m}$ mass flow rate, kg/s
- P exchange perimeter, m
- T temperature, K
- v_{wind} wind speed, m/s
- V exchange volume, m^3

Greek symbols

- λ thermal conductivity, $W/m/K$
- ρ density, kg/m^3

Subscripts and superscripts

- C Cold HTF
- eff Effective
- ext Exterior/Outdoor
- fin Fin
- H Hot HTF

in In

l Liquid phase

m Melting

out Out

PCM PCM

s Solid phase

sol Solar

References

[1] International Energy Agency. *Energy Efficiency: Buildings the global Exchange for Energy Efficiency Policies, Data and Analysis*. IEA Publications; 2021 Nov. Technical Report No.: Energy Efficiency 2021.

[2] Dincer I. *On thermal energy storage systems and applications in buildings*. Energy Build. 2002 May 1;34(4):377–88.

[3] Zalba B, Marin JM, Cabeza LF, Mehling H. *Review on thermal energy storage with phase change: materials, heat transfer analysis and applications*. Appl Therm Eng. 2003 Feb 1;23(3):251–83.

[4] Devaux P, Farid MM. *Benefits of PCM underfloor heating with PCM wallboards for space heating in winter*. Appl Energy. 2017 Apr 1;191:593–602.

[5] Stritih U. *An experimental study of enhanced heat transfer in rectangular PCM thermal storage*. Int J Heat Mass Transf. 2004 Jun 1;47(12):2841–7.

[6] Du K, Calautit J, Wang Z, Wu Y, Liu H. *A review of the applications of phase change materials in cooling, heating and power generation in different temperature ranges*. Appl Energy. 2018 Jun 15;220:242–73.

[7] Faraj K, Khaled M, Faraj J, Hachem F, Castelain C. *A review on phase change materials for thermal energy storage in buildings: Heating and hybrid applications*. J Energy Storage. 2021 Jan 1;33:101913.

[8] Seddegh S, Wang X, Henderson AD, Xing Z. *Solar domestic hot water systems using latent heat energy storage medium: A review*. Renew Sustain Energy Rev. 2015 Sep 1;49:517–33.

[9] Jin X, Zhang H, Huang G, Lai ACK. *Experimental investigation on the dynamic thermal performance of the parallel solar-assisted air-source heat pump latent heat thermal energy storage system*. Renew Energy. 2021 Dec 1;180:637–57.

[10] Zhou D, Zhao CY, Tian Y. *Review on thermal energy storage with phase change materials (PCMs) in building applications*. Appl Energy. 2012 Apr 1;92:593–605.

[11] Martinez RG, Goikolea BA, Paya IG, Bonnamy P, Raji S, Lopez J. *Performance assessment of an unglazed solar thermal collector for envelope retrofitting*. Energy Procedia. 2017 Jun 1;115:361–8.

[12] Bonnamy P, Raji S, Lopez J, Garay R. *Expérimentation et modélisation d'un collecteur solaire opaque pour préchauffage de l'eau*. In: Kjelstrup S., Hustad E., Gundersen T., Røsjorde A., Tsatsaronis G., editors. ECOS 2005: Proceedings of the 18th International Conference on Efficiency, Cost, Optimization, Simulation, and Environmental Impact of Energy Systems; 2016 Jun 20-25; Trondheim, Norway. Tapir Academic Press:777-84.

[13] Nobatek/INEF 4. *BATISOL: Capteurs solaires thermiques - solutions Nobatek/INEF 4* Available at: `https://www.nobatek.inef4.com/batisol/` [accessed 03.09.2023].

[14] Dimaano MNR, Watanabe T. *The capric–lauric acid and pentadecane combination as phase change material for cooling applications*. Appl Therm Eng. 2002 Mar 1;22(4):365–77.

[15] Bouzouidja R, Aketouane Z, Lhomer R, Varela B, Cruz JL, Serra S, Reneaume J.M., Sempey A. *Choice of the Suitable Melting Temperature of Phase Change Material: Application on Solar Assisted Heat Pump*. In: 2022 IEEE 10th International Conference on Smart Energy Grid Engineering (SEGE). 2022. p. 58–62.

[16] Kauranen P, Peippo K, Lund PD. *An organic PCM storage system with adjustable melting temperature*. Sol Energy. 1991 Jan 1;46(5):275–8.

https://doi.org/10.52202/069564-0189